Technical Update on MR Neurography

Teodoro Martín-Noguerol, MD[1] Paula Montesinos, PhD[2] Alvand Hassankhani, MD[3]
Dario A. Bencardino, FY[4] Rafael Barousse, MD[5] Antonio Luna, MD, PhD[1]

[1] MRI Unit, Radiology Department, HT Médica, Jaén, Spain
[2] Clinic Scientist, Philips Healthcare, Madrid, Spain
[3] Department of Radiology, Division of Neuroradiology, Perelman School of Medicine at the University of Pennsylvania, Philadelphia
[4] School of Liberal Studies, New York University, New York, New York
[5] Peripheral Nerve and Plexus Department, Centro Rossi, Buenos Aires, Argentina

Address for correspondence Teodoro Martín-Noguerol, MD, MRI Unit Radiology Department, HT Médica, Carmelo Torres 2, 23007 Jaén, Spain (e-mail: t.martin.f@htime.org).

Semin Musculoskelet Radiol 2022;26:93–104.

Abstract

Imaging evaluation of peripheral nerves (PNs) is challenging. Magnetic resonance imaging (MRI) and ultrasonography are the modalities of choice in the imaging assessment of PNs. Both conventional MRI pulse sequences and advanced techniques have important roles. Routine MR sequences are the workhorse, with the main goal to provide superb anatomical definition and identify focal or diffuse nerve T2 signal abnormalities. Selective techniques, such as three-dimensional (3D) cranial nerve imaging (CRANI) or 3D NerveVIEW, allow for a more detailed evaluation of normal and pathologic states. These conventional pulse sequences have a limited role in the comprehensive assessment of pathophysiologic and ultrastructural abnormalities of PNs. Advanced functional MR neurography sequences, such as diffusion tensor imaging tractography or T2 mapping, provide useful and robust quantitative parameters that can be useful in the assessment of PNs on a microscopic level. This article offers an overview of various technical parameters, pulse sequences, and protocols available in the imaging of PNs and provides tips on avoiding potential pitfalls.

Keywords
- peripheral nerve
- neurography
- magnetic resonance imaging

The clinical and imaging evaluation of the peripheral nerves (PNs) is challenging. The small size, tortuous course, location (commonly in the vicinity of vessels or in close proximity to fibro-osseous tunnels), and nonspecific clinical manifestations of peripheral neuropathies are among the many challenges that radiologists face when confronted with PN imaging.[1] Both ultrasonography (US) and magnetic resonance imaging (MRI)[2] are useful in the evaluation of the PNs. Setting aside the advantages and disadvantages of MRI and US, the assessment of PNs using conventional MRI sequences is insufficient. A more comprehensive assessment of the PNs requires selective MRI sequences for proper identification, detection, and characterization of PN disorders. In the past 20 years, magnetic resonance neurography (MRN) techniques now allow a more meticulous depiction of the PNs. Advanced MR techniques provide useful insights into their pathophysiology.[3] We briefly review conventional nonselective and advanced pulse sequences used in PN imaging, focusing on various protocols and technical adjustments aimed at optimizing image quality.

Magnets and Coils

Magnetic field strength and proper coil selection remain essential in the evaluation of PNs. In general, 3 T is preferred because it provides a higher signal-to-noise ratio (SNR) at a faster pace, particularly important with three-dimensional (3D) sequences; however, high-resolution images can also be obtained on 1.5-T field strength magnets with upgraded software. Two-dimensional (2D) sequences are almost equally competitive at 1.5 T and 3 T. But when working at 3 T, other facts must be considered. Artifacts derived from B0 magnetic field inhomogeneity, fat suppression problems, or susceptibility artifacts can be more pronounced on 3 T. To combat such problems, specific sequences were developed to

Issue Theme Imaging Evaluation of Nerves; Guest Editor, Jenny T. Bencardino, MD

© 2022. Thieme. All rights reserved.
Thieme Medical Publishers, Inc., 333 Seventh Avenue, 18th Floor, New York, NY 10001, USA

DOI https://doi.org/10.1055/s-0042-1742753.
ISSN 1089-7860.

This document was downloaded for personal use only. Unauthorized distribution is strictly prohibited.

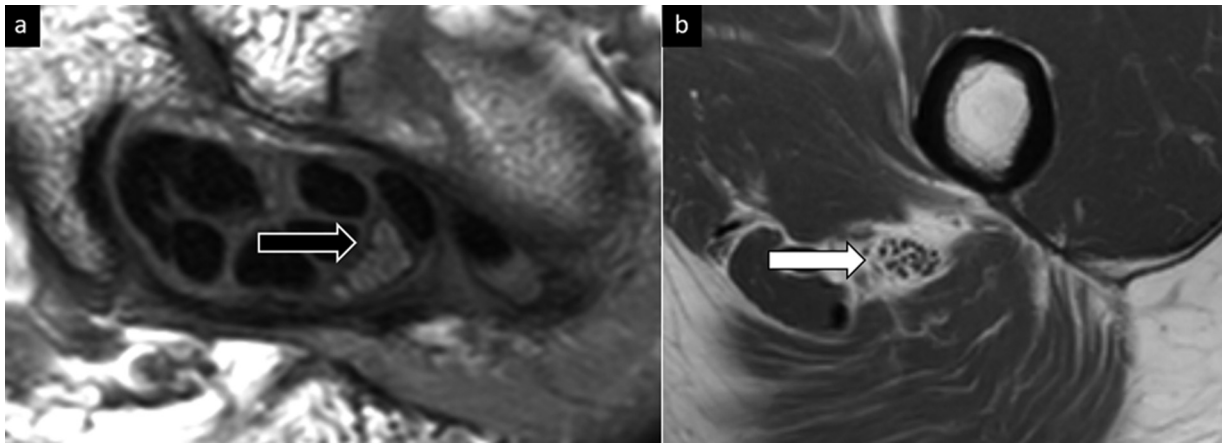

Fig. 1 T1-weighted (T1W) sequence for the assessment of peripheral nerves. T1W images provide exquisite anatomical details. (**a**) Axial T1W of the wrist for assessment of the median nerve (black arrow) in a 24-year-old male health volunteer. (**b**) Axial T1W of the thigh for assessment of the sciatic nerve (white arrow) in a 75-year-old male health volunteer. Note the intra-fascicle fat between the nerve bundles.

achieve high-resolution images while mitigating fat or tissue suppression artifacts.[4,5] When imaging near metallic hardware, 1.5 T is preferred because susceptibility artifacts are less conspicuous.[6,7]

Certain technical factors, such as field of view (FOV), should be tailored to the specific anatomical region of interest. Proper coil selection is also important. For example, phased array head coils are preferred for the imaging of the cranial nerves, and dedicated extremity coils should be used when imaging the PNs in the extremities to achieve higher SNR and spatial resolution. For plexus imaging, a combination of coils may be needed to achieve higher and more homogeneous signal.[6,7]

Nonselective MRI Sequences for Assessment of Peripheral Nerves

Despite the latest advances of MRN, conventional nonselective MRI sequences are of utmost importance in the assessment of PNs. The tissue contrast and the anatomical information provided by these sequences aid in identifying various PN pathologies. These sequences provide adequate spatial resolution to discriminate between PNs and adjacent structures, such as muscles, bone, or ligaments. The use of high-resolution 2D morphological MRI sequences with dedicated FOV provides excellent anatomical resolution for the assessment of PN fascicles, especially in pathologic

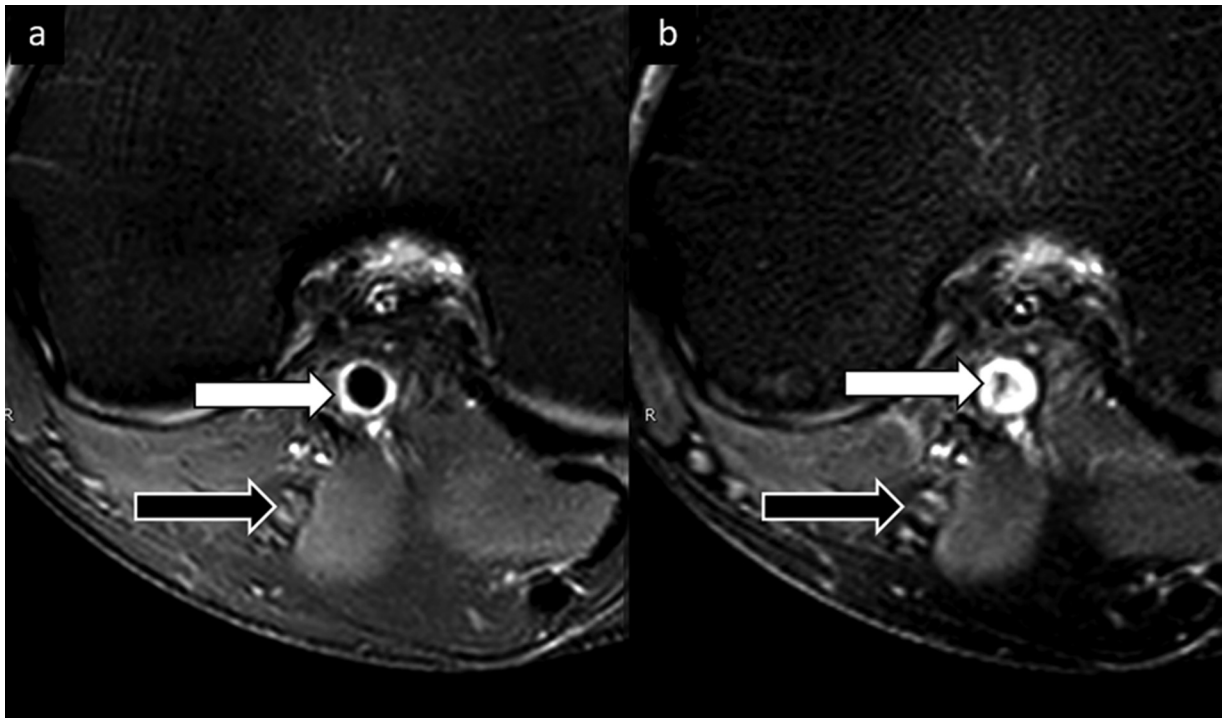

Fig. 2 Examples of T2 fat suppression techniques. (**a**) Axial T2 spectral adiabatic inversion recovery (SPAIR) and (**b**) axial short tau inversion recovery (STIR) of the knee in a healthy volunteer. The black arrow indicates the common tibial nerve. Note the higher signal-to-noise ratio and lower flow artifact from the popliteal vessels (white arrow) in SPAIR as compared with STIR.

 © 2022. Thieme. All rights reserved.

This document was downloaded for personal use only. Unauthorized distribution is strictly prohibited.

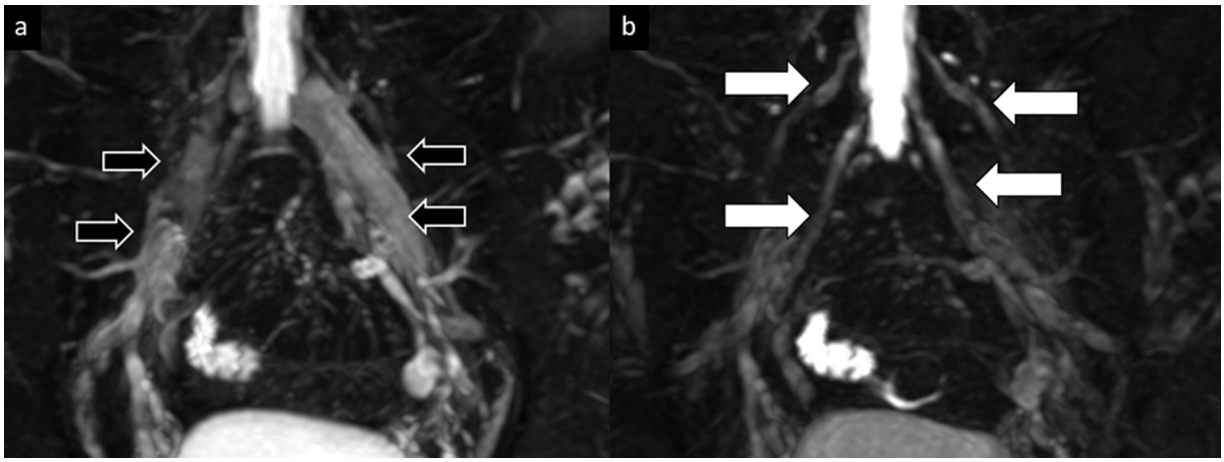

Fig. 3 Acquisition of short tau inversion recovery (STIR) sequences after gadolinium-based contrast agent (GBCA) administration in a 57-year-old man who underwent a lumbar plexus study for chronic pubalgia. (**a**) Coronal maximum intensity projection (MIP) image of the STIR sequence for assessment of the lumbar plexus. Note the dominance of the iliac vessels (black arrows) that hinder visualization of the lumbar nerve roots. (**b**) Coronal MIP image of STIR sequence acquired after GBCA administration. Note the suppression of signal intensity within the iliac vessels and better visualization of the lumbar nerve roots (white arrows).

conditions.[8] MR protocols for PN assessment should include a combination of anatomical and fluid-sensitive images.

The sequences available for PN assessment using conventional MRI sequences range from T1-weighted (T1W) images to T2-weighted (T2W) images.[9,10] T1W sequences can provide exquisite anatomical information (►**Fig. 1**). In general, fast spin-echo/turbo spin-echo (FSE/TSE) sequences are used. Spatial resolution and tissue contrast between surrounding fat and PN fascicles (that are also surrounded by fat) provided by T1W images are essential for anatomical evaluation of PNs. T2W images are usually acquired combined with fat suppression techniques. PNs have longer T2 relaxation times compared with muscles and are often surrounded by fat. These higher T2 relaxation times, combined with strong fat suppression, generate images with good nerve-to-background contrast, in which abnormal signal intensities in the nerves are easily identified. Preferred sequences are FSE/TSE sequences with high TE values, to maximize contrast with muscle.[11]

This fat suppression can be achieved either with a short tau inversion recovery (STIR) technique or with a spectral approach, such as spectral presaturation with inversion recovery or spectral attenuated inversion recovery (SPAIR) (►**Fig. 2**). STIR sequences usually enable a more homogeneous uniform fat suppression in large FOV, such as the brachial or lumbar plexus. However, STIR images usually have a lower SNR when compared with T2W SPAIR. The latter is recommended for smaller FOV or assessment of localized neuropathies.[12] At 3 T, SPAIR is generally preferred because it provides a more homogeneous fat suppression and higher SNR. The differentiation between PNs and the adjacent vascular bundles (especially low-flow veins) is challenging on STIR. Some authors have proposed acquisition of STIR sequences after gadolinium-based contrast agents (GBCAs) to reduce or suppress the signal from adjacent vessels, with promising results[13] (►**Fig. 3**). ►**Table 1** summarizes the recommended parameters of a clinical routine protocol for PN assessment.

Fat suppression using Dixon reconstruction technique is also valuable in the imaging of PNs. Dixon-based techniques exploit the differences in chemical-shift frequencies between water and fat, allowing separation of fat and water

Table 1 Conventional MRI protocol for peripheral nerve assessment

	T1 TSE	T2W TSE	T2W SPAIR	3D STIR
TR/TE, ms	550/15	3,000/90	3,500/80	2,200/260
FOV, mm	400 × 250 × 80	400 × 250 × 80	400 × 250 × 80	250 × 400 × 170
Slice thickness/slice gap, mm	3/1.2	3/1.2	3/1.2	2/− 1
Acquired voxel size, mm	0.8 × 1	0.8 × 1	0.95 × 1.2	1.2 × 1.2 × 2
Reconstructed voxel size, mm	0.56 × 0.56	0.69 × 0.69	0.69 × 0.69	0.6 × 0.6 × 1
Fat saturation	No	No	SPAIR	STIR (TI = 220 ms)
SENSE acceleration factor	No	No	No	3 × 1.5
Acquisition time, min:s	~ 4:00	~ 4:00	~ 4:00	~ 6:00

Abbreviations: 3D, three-dimensional; FOV, field of view; MRI, magnetic resonance imaging; SPAIR, spectral adiabatic inversion recovery; STIR, short tau inversion recovery; T2W, T2-weighted; TSE, turbo spin echo.
Note: FOV and spatial resolution should be adapted based on the region under study.

 © 2022. Thieme. All rights reserved.

This document was downloaded for personal use only. Unauthorized distribution is strictly prohibited.

signals from in-phase and opposed-phase images.[14] This technique allows a more homogeneous fat suppression, usually better than STIR or SPAIR. Dixon technique can be applied on spin-echo and gradient-echo sequences. However, in MRN, Dixon is usually applied to 2D FSE/TSE pulse sequences (►**Fig. 4**). ►**Table 2** summarizes the recommended parameters for acquisition of T1W and T2W Dixon sequences for PN assessment.

The 3D FSE/TSE acquisitions have been successfully improved with new MRI advances, such as modulated refocusing flip angles, longer echo train lengths, and acceleration techniques, such as parallel imaging or the more recent compressed sensing methodology.[15] In recent decades, other technological improvements in the design of MRI systems have allowed the development of advanced 3D neurography morphological sequences. These sequences provide the highest spatial resolution for PN assessment. As mentioned earlier, 3D sequences combine very high-resolution acquisitions with excellent SNR at 3 T. This approach enables isotropic acquisitions that will later allow for multiplanar reconstructions.[16]

Gadolinium and Peripheral Nerves

PNs should not enhance if the blood-neural barrier (BNB) is intact, and gadolinium has a limited role in the imaging assessment of PN disease. The most common indications for administration of contrast are in the assessment of primary or metastatic neoplasms, infections, and inflammatory diseases

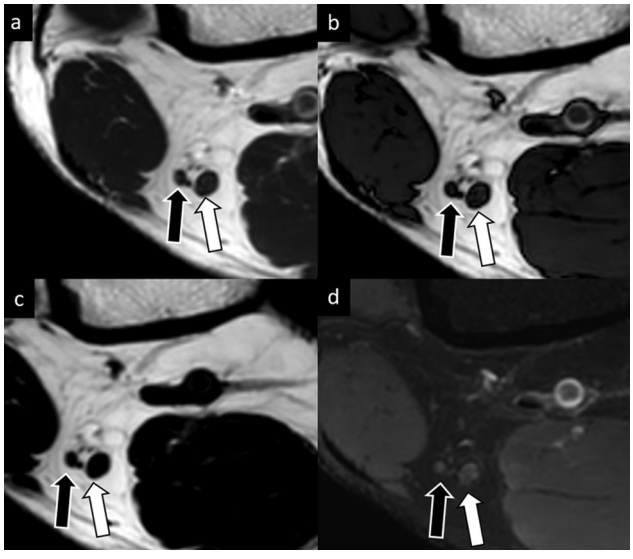

Fig. 4 T2 Dixon turbo spin-echo (TSE) sequence of the knee for common tibial nerve (white arrow) and common peroneal nerve (black arrow) assessment on a 32-year-old healthy volunteer female T2 Dixon sequence provides four sets of images from one single acquisition. (**a**) T2 Dixon in-phase image, with similar contrast to conventional T2 TSE/fast spin-echo sequences. (**b**) T2 Dixon out-of-phase (or opposed-phase) image, with its characteristic Indian ink artifact due to signal cancellation of voxels located in the interphase between fat and water. (**c**) T2 Dixon fat-only image, in which all the not-containing fat voxels are canceled. (**d**) T2 Dixon water-only image, equivalent to a conventional T2 fat-saturated or short tau inversion recovery sequence but with a higher signal-to-noise ratio and more homogeneous fat suppression.

Table 2 Dixon parameters for peripheral nerve assessment

	T1 TSE Dixon	T2 TSE Dixon
TR/TE, ms	630/7	3,000/90
FOV, mm	$200 \times 200 \times 100$	$200 \times 200 \times 100$
Slice thickness/ slice gap, mm	3/1.2	3/1.2
Acquired voxel size, mm	0.69×0.9	0.65×0.8
Reconstructed voxel size, mm	0.6×0.6	0.6×0.6
SENSE acceleration factor	1.5	1.5
Acquisition time, min	$\sim$ 4:30	$\sim$ 4:00

Abbreviations: FOV, field of view; TSE, turbo spin echo.
Note: FOV and spatial resolution should be adapted based on the region under study.

that may disrupt BNB integrity. Note that severe trauma may also result in BNB damage, but the role of contrast administration in the setting of trauma is not fully established[3,17] (►**Fig. 5**). Postcontrast T1W with fat suppression (usually spectral fat suppression) or T1 Dixon water-only images can depict gadolinium uptake in diseased nerves and differentiate abnormal enhancement from normal high intensity of perineural or even intraneural fat.

Dynamic contrast-enhanced (DCE)-MR perfusion may have a role in the evaluation of PNs. DCE-MRI sequences are acquired immediately after contrast injection and enable evaluation of the microvascular environment surrounding the PNs. ►**Table 3** summarizes the protocol parameters for DCE-MR perfusion. These types of sequences have high temporal resolution that allows radiologists to assess the pass of GBCAs through the capillary network, detecting contrast uptake and signal changes within PNs. These sequences are part of state-of-the-art MRI protocols in the assessment of lesions in many organs, such as brain, prostate, breast, or liver.

The added value of DCE-MRI for PN assessment is related to the pathophysiologic information provided in terms of parameters derived such as Ktrans, Kep, Ve, Vp, wash-in, or wash-out rates. These parameters may allow noninvasive ways of differentiating nonaggressive, probably benign, lesions from more aggressive malignancies. In addition, these parameters can provide certain quantitative threshold values useful in follow-up or treatment response. MR signal intensity of either a single voxel or region of interest can be plotted over acquisition time, generating time intensity curves (TICs) or signal-time curves. TICs reflect the changes in T1 signal intensity with the pass of GBCAs through the capillary network. The shape and characteristics of TICs are another physiologic parameter that helps assess lesion aggressiveness[18] (►**Fig. 6**). The acquisition of DCE-MRI sequences immediately after GBCAs injection does not influence the later acquisition of conventional gadolinium-enhanced T1W (with or without fat suppression) for routine assessment of GBCA uptake by PNs.

 © 2022. Thieme. All rights reserved.

This document was downloaded for personal use only. Unauthorized distribution is strictly prohibited.

Table 3 Dynamic contrast-enhanced MRI parameters for peripheral nerve lesion assessment

	1.5 T	3 T
TE/TR, ms	2.1/6	1.3 / 4.0
Flip angle, degrees	10	10
FOV, mm	190	190
Matrix	112 × 149	112 × 96
Voxel, mm	1.17 × 2.40	1.90 × 2.30
Thickness, mm	7	3.5
Dynamic time, s	5	5
N° dynamics	50	50
Acquisition time, min:s	4:00	4:00

Abbreviations: FOV, field of view; MRI, magnetic resonance imaging.
Note: FOV and spatial resolution should be adapted based on the region under study.

Magnetic Resonance Neurography

Morphological MR Neurography

Recent advances in high-field gradients and coil design have led to the development of advanced 3D neurography sequences, some of which are summarized here.

Three-dimensional Cranial Nerve Imaging

Three-dimensional cranial nerve imaging (3D CRANI) is a sequence intended for the visualization of the extraforaminal cranial nerves. Imaging of the extracranial nerves is challenging due to their small diameter, complex shape, and the potential presence of artifacts caused by motion, susceptibility, fat suppression, and magnetic field inhomogeneities. The 3D CRANI is a black-blood 3D STIR TSE sequence that uses pseudo steady-state (PSS) sweep in combination with a motion-sensitized driven equilibrium (MSDE) pulse.[19] The combination of MSDE and STIR enables better fat suppression and reduces signal from muscle, and blood across the FOV. Additionally, the PSS sweep is designed to keep the signal strength constant. Compressed sensing and other acceleration techniques can supplement this sequence to reduce acquisition time. Maximum intensity projections (MIPs) and plane reformats can be applied for better visualization of the evaluated nerve trajectory (►**Fig. 7**).[5] ►**Table 4** summarizes the protocol parameters for 3D CRANI acquisition.

Three-dimensional NerveVIEW

Three-dimensional NerveVIEW is a high-resolution 3D STIR sequence with a large bandwidth that allows improved fat suppression in a higher range of frequencies. The addition of MSDE pulse results in dephasing of the moving spins, nulling out unwanted signal from blood vessels that run parallel to the nerves[16] and reducing the intralumen signal of vessels. This technique is especially useful in the evaluation of the brachial and lumbar plexus, overcoming fat suppression challenges and flow-related artifacts (►**Fig. 8**). In addition, the 3D isotropic imaging method allows for reformats in any plane (including oblique) without loss of resolution, improving visualization of intricate spinal nerves. Protocol details and acquisition parameters are listed in ►**Table 5**.

Three-dimensional Diffusion-weighted Imaging-PSIF

The 3D diffusion-weighted imaging-PSIF is a balanced gradient-echo steady-state free precession sequence that has less influence on local magnetic field inhomogeneity due to encompassing features of spin-echo pulse sequence.[20] It can be performed with or without fat suppression, although

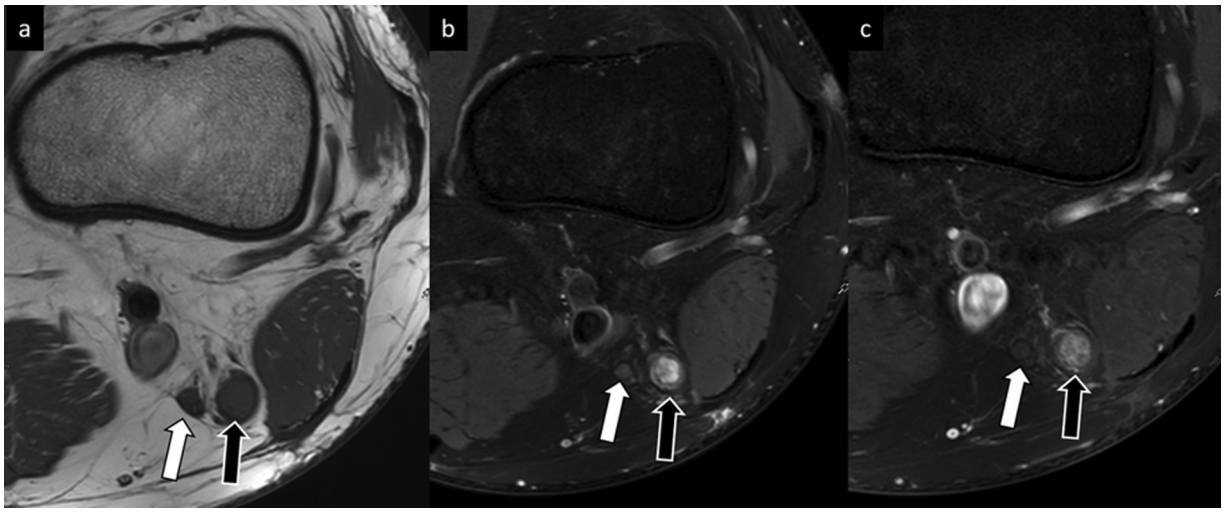

Fig. 5 Use of gadolinium-based contrast agents for the assessment of peripheral nerve lesions. A 45-year-old man with a recent left knee sprain refers for left foot drop. (**a**) Axial T1-weighted turbo spin echo shows enlargement of the common peroneal nerve (black arrow) compared with the normal common tibial nerve (white arrow). (**b**) Axial T2 spectral adiabatic inversion recovery (SPAIR) shows an increase of signal intensity within the common peroneal nerve (black arrow) with normal signal intensity within the common tibial nerve (white arrow). (**c**) Axial T1 SPAIR after gadolinium administration demonstrates intense common peroneal nerve enhancement (black arrow) compared with an absence of enhancement within the common tibial nerve (white arrow). The use of T1 fat suppression sequences such as SPAIR increases the conspicuity of enhancement. The enhancement within the common peroneal nerve suggests disruption of the blood-nerve barrier.

 © 2022. Thieme. All rights reserved.

This document was downloaded for personal use only. Unauthorized distribution is strictly prohibited.

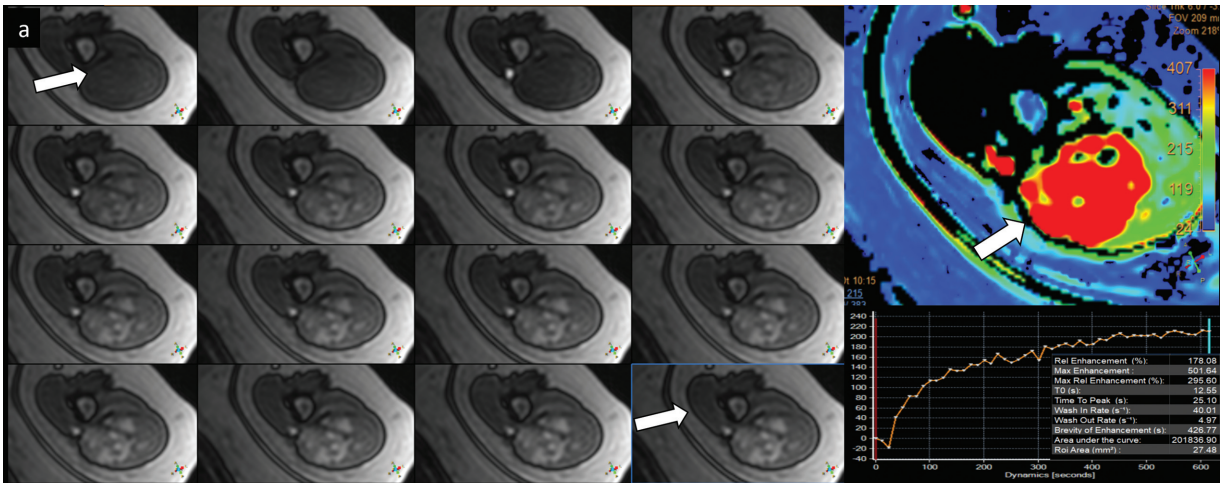

Fig. 6 Radial nerve schwannoma in a 45-year-old woman. Dynamic contrast-enhanced magnetic resonance imaging perfusion is useful in assessing the microvascular environment. (**a**) The acquisition of multiple consecutive images within the first minutes after gadolinium administration allows distribution of gadolinium-based contrast agents through the capillary network of the peripheral nerves (white arrows). This approach is especially relevant in the characterization of benign versus malignant lesions. (**b**) Parametric maps and (**c**) the time intensity curve are useful in lesion characterization.

selective water excitation–type fat suppression is recommended for a better nerve-to-background contrast ratio.[4]

Vascular signal is suppressed due to the steady-state nature of this sequence and the use of a low diffusion moment, combined with intrinsic T2 nerve hyperintensity resulting in nerve-selective imaging. The 3D DWI-PSIF is acquired with submillimeter isotropic resolution.[21] Acquired images can be reformatted in any arbitrary plane, and MIPs may be used to improve nerve visualization.[22] Recommended parameters for a 3-T 3D DWI-PSIF sequence are summarized in ►**Table 6**.[4]

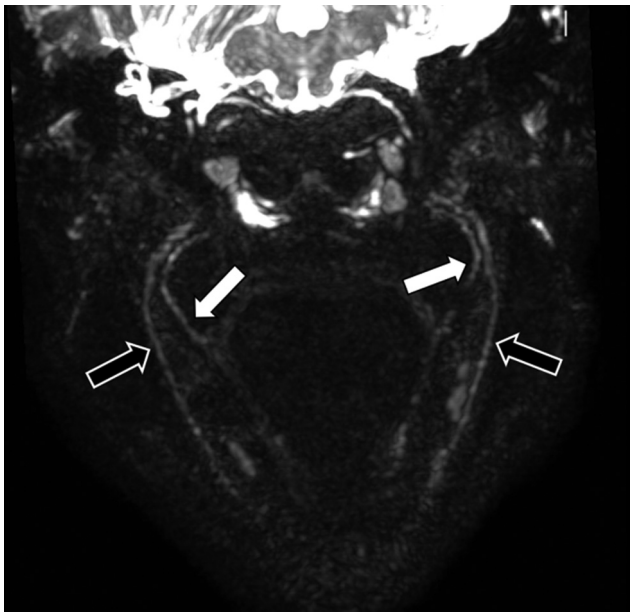

Fig. 7 Three-dimensional cranial nerve imaging sequence for the extracranial assessment of cranial nerves in a healthy 48-year-old woman. Coronal oblique reconstruction of maximum intensity projection multiplanar reformation demonstrates proper visualization of both lingual (white arrows) and inferior alveolar nerves (black arrows).

Functional MR Neurography Sequences

In the last decade, new MRI sequences have been incorporated that provide higher resolution assessment of the PNs. Most of these sequences have been imported from other anatomical areas, such as the central nervous system. These sequences enable radiologists to evaluate PNs beyond their morphological properties, providing valuable information on pathophysiology. The added value of these sequences is to provide quantifiable data, helping establish threshold values to discriminate between normal and pathologic conditions, for example disease grading or treatment monitoring.[23]

Diffusion-weighted Imaging Neurography

DWI allows in vivo detection and quantification of water molecule movement. As in other anatomical areas, the most common DWI technique is single-shot echo-planar imaging

Table 4 Parameters for three-dimensional cranial nerve imaging sequence acquisition

TR/TE, ms	2,300/150
FOV, mm	200 × 200 × 100
Slice thickness/slice gap, mm	0.5/− 0.45
Acquired voxel size, mm	0.9 × 0.9 × 0.9
Reconstructed voxel size	0.5 × 0.5 × 0.45
Slice oversampling	1.5
BB pulse	MSDE
Fat saturation	STIR
SENSE acceleration factor	2 × 1.2
Acquisition time, min:s	~ 8:00

Abbreviations: BB, black blood; FOV, field of view; MSDE, motion-sensitized driven equilibrium; STIR, short tau inversion recovery; TSE, turbo spin echo.
Note: FOV and spatial resolution should be adapted based on the region under study.

 © 2022. Thieme. All rights reserved.

This document was downloaded for personal use only. Unauthorized distribution is strictly prohibited.

Fig. 8 Three-dimensional (3D) NerveVIEW for assessment of the lumbar plexus in a healthy 57-year-old woman. (**a**) Coronal T2 spectral adiabatic inversion recovery of the pelvis for lumbar plexus evaluation shows multiple hyperintense structures that correspond with lumbar plexus roots and sciatic nerves (white arrows). Note that the adjacent pelvic and gluteal vessels (black arrows) may hinder optimal visualization of peripheral nerves (PNs). (**b**) The 3D NerveVIEW suppresses the signal from vascular structures and increases the conspicuity of the PNs.

(EPI). This sequence is robust, fast, and commonly available. The intrinsic structure of PNs facilitate water movement along its long axis and restrict water diffusion along its short axis. Thus diffusion motion-probing gradients are applied perpendicular to the long axis of the PNs. With proper background signal suppression, high contrast between PNs and the surrounding structures can be achieved (►**Fig. 9**).[24] Acquisition of at least two b-values is necessary to calculate the apparent diffusion coefficient (ADC). ADC indirectly measures the displacement of water molecules in extracellular space. ADC values are helpful in discriminating various pathologies. For example, in trauma the ADC values tend to be increased, due to associated edema or inflammation. Benign PN tumors, such as neurofibroma, schwannoma, or neuroma, usually show higher ADC values ($> 1.1 \times 10^{-3}$ mm^2/s) than malignant ones ($< 1.1 \times 10^{-3}$ mm^2/s). The optimal b-value for acquiring reliable DWI MRN of the PNs is between 600 and 800 s/mm^2.[25] ►**Table 7** summarizes the main parameters for acquisition of DWI neurography.

Table 5 Three-dimensional NerveVIEW parameters for peripheral nerve assessment

TR/TI/TE, ms	2,200/250/170
FOV, mm	$300 \times 390 \times 170$
Slice thickness/slice gap, mm	$2/-1$
Acquired voxel size, mm	$1.2 \times 1.2 \times 2$
Reconstructed voxel size, mm	$0.6 \times 0.6 \times 1$
Slice oversampling	1.5
BB pulse	MSDE
Fat saturation	STIR
SENSE acceleration factor	3×1.3
Acquisition time, min	~ 6:00

Abbreviations: BB, black blood; FOV, field of view; MSDE, motion-sensitized driven equilibrium; STIR, short tau inversion recovery; TSE, turbo spin echo.
Note: FOV and spatial resolution should be adapted based on the region under study.

Diffusion Tensor Imaging Neurography

Diffusion tensor imaging (DTI) is an advanced technique that can be useful in assessing functional neurography of the PNs. DTI determines a dominant direction in the movement of water molecules along the axon by using motion-probing gradients in multiple directions.[26,27] This type of diffusion is

Table 6 PSIF parameters for peripheral nerve assessment

TR/TE, ms	10/2.47
FOV, mm	$100–320 \times 100$
Slice thickness/ slice gap, mm	0.9
Effective voxel size, mm	$0.7–0.8 \times 0.7–0.8 \times 0.7–0.8$
b-value, s/mm^2	80–90
Matrix size, mm	$120–420 \times 100–120$
Fat suppression	Water excitation normal
Acquisition time, min:s	4:30–6:25

Abbreviation: FOV, field of view.
Note: FOV and spatial resolution should be adapted based on the region under study.

 © 2022. Thieme. All rights reserved.

This document was downloaded for personal use only. Unauthorized distribution is strictly prohibited.

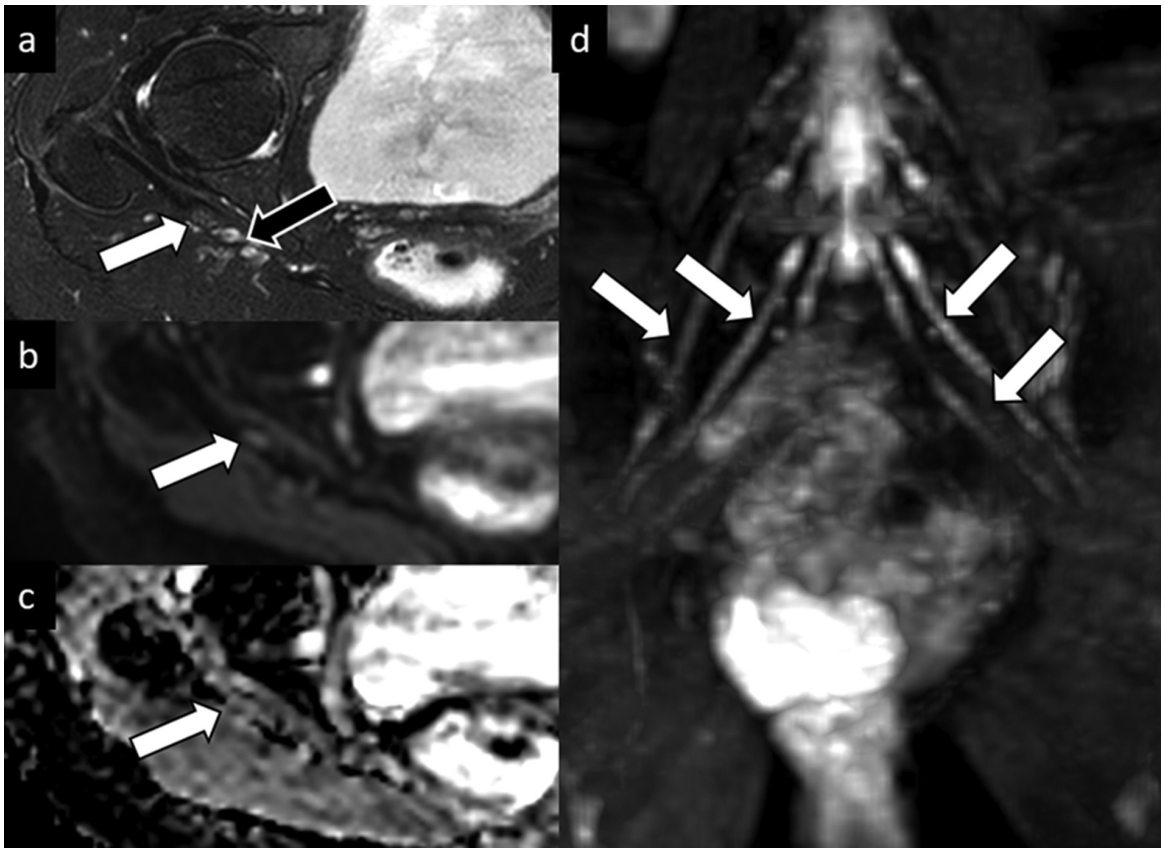

Fig. 9 Diffusion-weighted imaging (DWI) neurography of the sciatic nerve and lumbar plexus in a healthy 44-year-old woman. (**a**) Axial short tau inversion recovery shows the neurovascular bundle at the right greater sciatic notch with sciatic nerve (white arrow) and gluteal vessels (black arrow). (**b**) Axial b-value 800 DWI neurography demonstrates only the sciatic nerve as an hyperintense structure due to the restriction of water diffusion on the axial plane inside the nerve (white arrow). Note the loss of signal intensity from vessels because of the diffusion gradients. (**c**) Apparent diffusion coefficient map derived from DWI enables quantification of water movement in the extracellular space (1.4×10^{-3} mm^2/s). (**d**) Coronal maximum intensity projection reconstruction of DWI neurography of the lumbar plexus depicts the lumbar roots (arrows) with high contrast against background structures. Judicious use of the fat suppression pulse technique and high-diffusion gradients are essential.

known as anisotropic and determined by the microstructure of the PN that facilitates movement of water molecules along the major axis of the nerve.[28,29] In DTI, the images are acquired in multiple directions to detect a dominant movement. DTI-based neurography provides various parameters, such as fractional anisotropy (FA), mean diffusivity (MD), axial diffusivity (AD), and radial diffusivity (RD), that may prove to be useful in determining the pathophysiology of PNs.

Table 7 Diffusion-weighted imaging neurography parameters for peripheral nerve assessment

	1.5 T	3.0 T
TR/TE, ms	15,233/65	2,179/72
Flip angle, degrees	90	90
FOV, mm	130	130
Voxel, mm	1.55/1.55/4.00	1.55/1.55/4.00
Thickness, mm	4	3
b-values, s/mm^2	0, 800	0, 800
Acquisition time, min:s	3:30	2:50

Abbreviation: FOV, field of view.
Note: FOV and spatial resolution should be adapted based on the region under study.

FA, which ranges between 0 and 1, is considered the most sensitive parameter in the evaluation of PNs and an index of fascicular organization. FA was found to be decreased when there is loss of such neural organization.[30] MD (mm^2/s) is somewhat similar to ADC but provides greater precision in free movement of the water molecules in the extracellular space. AD (mm^2/s) estimates the degree of free movement of water molecules along the major axis of the nerve, thus reflecting the degree of axonal conduction.[31] RD (mm^2/s) can be considered the most specific indicator of myelin integrity because it estimates the free movement of water molecules along the short axis of the nerve. Increase in RD is found in conditions that involve myelin damage, such as injury to the nerve sheaths. RD may be decreased when there is a remyelination repair.[32–35] Finally, DTI studies allow high-resolution 3D neurographic reconstructions that provide additional information on the morphological and functional characteristics of the PNs, as well as their relationship with neighboring structures including PN tumors (►**Fig. 10**). ►**Table 8** summarizes the main parameters for acquisition of DTI neurography studies.[36–40]

 © 2022. Thieme. All rights reserved.

This document was downloaded for personal use only. Unauthorized distribution is strictly prohibited.

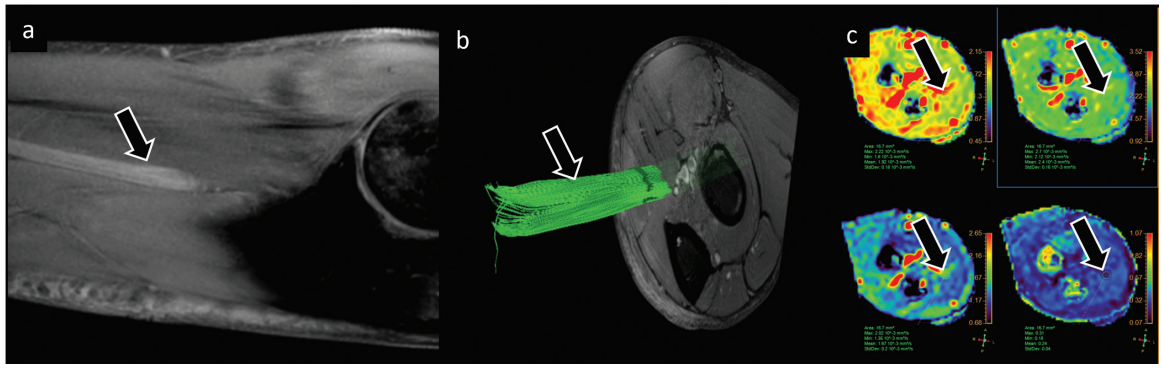

Fig. 10 Diffusion tensor imaging (DTI) neurography for radial nerve assessment in a healthy 21-year-old man. (a) Sagittal T2 spectral adiabatic inversion recovery shows the normal radial nerve along its long axis (black arrow). The application of multiple motion sensitizing gradient DTI sequence allows to represent (b) radial nerve (black arrow) using fiber tracking techniques and to obtain (c) fractional anisotropy, mean diffusivity, radial diffusivity, or axial diffusivity parametric maps for quantification of the radial nerve diffusion features (black arrows).

Table 8 Diffusion tensor imaging neurography parameters for peripheral nerve assessment

	1.5 T	3.0 T
TR/TE, ms	3,210/110	2,500/75
Flip angle, degrees	90	90
FOV, mm	140	140
Voxel, mm	1.50/1.50/3.00	1.50/1.50/3.00
Thickness, mm	4	3
No. of directions	12	12
b-values, s/mm^2	0, 800	0, 800
Acquisition time, min:s	7:15	5:25

Abbreviation: FOV, field of view.
Note: FOV and spatial resolution should be adapted based on the region under study.

Table 9 T2 mapping parameters for peripheral nerve assessment

TE, ms	8, 16, 24, 32, 40, 48, 56, 64, 72, 80
TR, ms	2,000
FOV: AP × RL × FH, mm	16 × 16 × 44
Thickness, mm	3
Matrix, mm	360 × 324
Plane	Axial
Acquisition time, min:s	5:34

Abbreviations: AP, anterior/posterior; FH, foot/head; FOV, field of view; RL, right/left.
Note: FOV and spatial resolution should be adapted based on the region under study.

T2 Mapping

The T2 mapping sequences are widely used in radiology, especially in the field of cardiac and cartilage imaging.[41,42] These sequences quantify T2 relaxation times of tissues more accurately than conventional T2W. For this aim, a multi-echo T2 sequence must be acquired with a range of TEs, generally from low (10 ms) to high TE (120 ms). After acquisition, T2 relaxation times are calculated. Information provided by T2 mapping may be displayed in parametric maps that provide information about the distribution of T2 relaxation values within PNs. ►**Table 9** summarizes the main parameters for the acquisition of DWI neurography studies. T2 mapping techniques help determine myelin water fraction within PNs, estimating the myelin water compartment and intra/extracellular water compartments. Water molecules bound to myelin sheaths have a shorter T2 relaxation time than those located in the intra- or extracellular compartments. PNs with myelin damage show larger T2 relaxation times than normal. The differences in T2 relaxation times are due to the slow motion of water bound to macromolecules compared with free water molecules.

The added value of T2 mapping for PN evaluation is in the ability to identify subtle changes in T2 signal within apparent normal PNs, which may be considered as very sensitive but not a specific indirect sign of PN disease (edema, atrophy, or gliosis). Preliminary studies have explored the utility of T2 mapping in the assessment of PNs in the settings of chronic inflammatory demyelinating polyradiculoneuropathy and lumbar or cervical compressive radiculopathy (►**Fig. 11**). These studies showed higher T2 relaxation values in compressive neuropathy compared with normal nerves, emphasizing the potential role of this technique as an objective and reproducible way to evaluate PN pathologies.[43–47]

Pitfalls and Artifacts

Different artifacts affect MR neurographic images, especially at 3 T, which is more prone to susceptibility and chemical-shift artifacts, particularly with large FOVs. Incorrect and inhomogeneous fat suppression is the most common frequently seen of these chemical-shift artifacts. To minimize them, shimming must be optimized.[29] Other approaches to reduce B0 inhomogeneity or artifacts due to incomplete/poor fat suppression are to position the area of interest at isocenter or to perform real-time B0 corrections.

The magic angle effect is another source of diagnostic error because it may produce artifactual hyperintensities mimicking pathology. To minimize the magic angle effect, a

 © 2022. Thieme. All rights reserved.

This document was downloaded for personal use only. Unauthorized distribution is strictly prohibited.

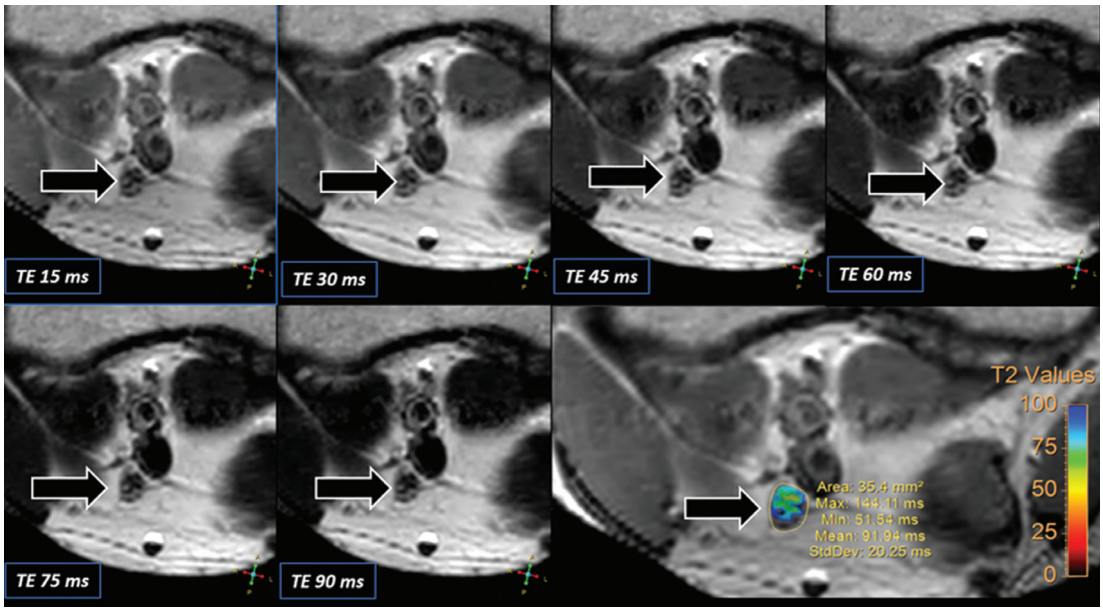

Fig. 11 T2 mapping for assessment of the common tibial nerve at the knee of a healthy 35-year-old man. The use of different TEs enables an estimation of the T2 signal intensity for each echo and calculates minimum (51.51 ms), maximum (144.11 ms), and mean (91.94 ms) T2 values for the common tibial nerve (black arrows).

high TE parameter should be used. Familiarity with this artifact is paramount to avoid misinterpretation of spurious intraneural T2 signal with disease.[48,49]

When DWI or DTI neurography studies are acquired, it is not uncommon to identify artifacts related to image distortion. In this scenario, the use of linear or nonlinear registration tools and gradient nonlinearity correction may help improve image quality. Inhomogeneity of the magnetic field due to the presence of air, bone, or blood products or foreign bodies presents a problem in single-shot EPI used for DTI acquisition. In the last decade, several non–EPI-based DTI sequences have been developed to minimize these artifacts. PROPELLER, multishot, and TSE DTI techniques are preferred when there is inhomogeneity in the magnetic field.[50] Non-EPI sequences may be useful when hematoma or foreign bodies are suspected in the setting of trauma or instrumentation.[51]

Physiologic motion artifacts, such as breathing or vascular pulsation, may be minimized using respiratory or cardiac gating. However, this approach increases the overall sequence acquisition time. Hyperintense flow-related intravascular signal can make a correct diagnosis challenging. Shorter echo train lengths and different phase-encoding gradients can help mitigate this problem. Specific neurographic sequences have incorporated different strategies including T2 prepulses to minimize vascular signal as a source of confusion.[52] Motion is another source of artifacts that directly degrades image quality. The use of acceleration techniques to reduce acquisition time is advised to improve patient experience and decrease motion.[6,53]

MR Neurography Protocols (When, Where, and How)

There are several clinical indications for performing MRN. Primary or secondary neuropathies including PN trauma or compressive neuropathies, tumor, infection, toxic-metabolic or inherited or autoimmune diseases may benefit from targeted MR protocols. Depending on the anatomical area or the peripheral nerve of interest, FOV and MR protocols should be adjusted to optimize the FOV and SNR. For example, assessment of brachial or lumbar plexopathy requires larger FOV than targeted assessment of a single PN in the extremities.

Whole-body MRN studies deserve a particular mention because of the large coverage required for multi-station (usually four to six) sequence acquisitions. Whole-body MRN studies are usually indicated for evaluation of diffuse polyneuropathies (usually inherited, paraneoplastic, or antibody mediated autoimmune) or for screening of PN tumors in the setting of systemic neurofibromatosis or schwannomatosis (►**Fig. 12**). Generally, whole-body MRN protocol does not differ from its use for oncologic indications, such as bone marrow assessment in multiple myeloma, bone metastasis detection, or lymphoproliferative disorders assessment. The basic MR protocol required for whole-body MRN studies should include DWI and coronal T2 fat suppression sequences, with acquisition time no longer than 20 minutes. If contrast is needed, coronal T1W with or without fat suppression should be acquired.

Radiology departments should have a basic and advanced MRN protocol for PN assessment. As described earlier, advanced MRN sequences need to be acquired when additional information about PNs is needed, such as in cases of apparent normal PN on conventional studies or when quantifiable parameters are necessary for treatment monitoring or establishing cutoff values between healthy and diseased nerves. The type, number, and order of MR sequences may vary depending on clinical suspicion and radiologist experience.

 © 2022. Thieme. All rights reserved.

This document was downloaded for personal use only. Unauthorized distribution is strictly prohibited.

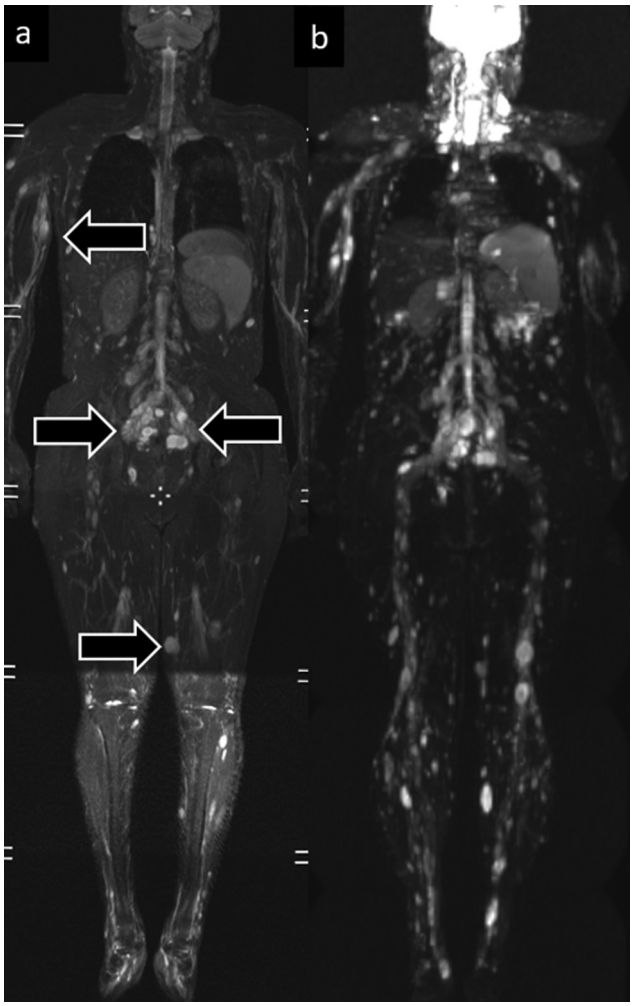

Fig. 12 Whole-body magnetic resonance neurography in a 25-year-old man with neurofibromatosis type 1. (**a**) Coronal short tau inversion recovery sequence of the whole body acquired with five stations identifies multiple neurofibromas (black arrows). (**b**) Coronal diffusion-weighted imaging maximum intensity projection (also acquired with a five-station strategy) increases the conspicuity of the lesions due to hypercellularity, noting multiple nodular masses along the brachial and lumbar plexus in the distribution of peripheral nerves in the upper and lower extremities.

Conclusion

A wide armamentarium of MR sequences is available for evaluation of PNs. MR neurographic protocols range from routine evaluation using conventional MR imaging focusing on morphological assessment, to advanced MR sequences that provide valuable information on the pathophysiology of the PNs. Advanced MRI sequences, such as 3D CRANI, NerveVIEW, DWI, DTI, or T2 mapping, require specific technical parameters to optimize image quality and to ensure reproducibility. New technical upgrades in the field of MRN are helpful to minimize artifacts and improve visualization of PNs. Depending on the PN or the anatomical region to evaluate, dedicated protocols, sequence selection, and study planning are needed.

Conflict of Interest
Antonio Luna is an occasional lecturer for Philips, Siemens Healthineers, Bracco, and Canon, and he receives royalties as a book editor from Springer. The remaining authors have no conflicts to declare. Paula Montesinos is a Philips employee.

References

1 Holzgrefe RE, Wagner ER, Singer AD, Daly CA. Imaging of the peripheral nerve: concepts and future direction of magnetic resonance neurography and ultrasound. J Hand Surg Am 2019; 44(12):1066–1079
2 Marquez Neto OR, Leite MS, Freitas T, Mendelovitz P, Villela EA, Kessler IM. The role of magnetic resonance imaging in the evaluation of peripheral nerves following traumatic lesion: where do we stand? Acta Neurochir (Wien) 2017;159(02):281–290
3 Ohana M, Moser T, Moussaouï A, et al. Current and future imaging of the peripheral nervous system. Diagn Interv Imaging 2014;95(01):17–26
4 Chhabra A, Subhawong TK, Bizzell C, Flammang A, Soldatos T. 3T MR neurography using three-dimensional diffusion-weighted PSIF: technical issues and advantages. Skeletal Radiol 2011;40 (10):1355–1360
5 Van der Cruyssen F, Croonenborghs TM, Hermans R, Jacobs R, Casselman J. 3D cranial nerve imaging, a novel MR neurography technique using black-blood STIR TSE with a pseudo steady-state sweep and motion-sensitized driven equilibrium pulse for the visualization of the extraforaminal cranial nerve branches. AJNR Am J Neuroradiol 2021;42(03):578–580
6 Chhabra A, Madhuranthakam AJ, Andreisek G. Magnetic resonance neurography: current perspectives and literature review. Eur Radiol 2018;28(02):698–707
7 Chhabra A, Andreisek G, Batra K. Magnetic resonance neurography interpretation. In: Chhabra A, Andreisek G, eds. Magnetic Resonance Neurography. New Delhi, India: JayPee Brothers Medical Publishers; 2012:23–36
8 Chhabra A, Flammang A, Padua A Jr, Carrino JA, Andreisek G. Magnetic resonance neurography: technical considerations. Neuroimaging Clin N Am 2014;24(01):67–78
9 Cejas C, Escobar I, Serra M, Barroso F. High resolution neurography of the lumbosacral plexus on 3T magnetic resonance imaging [in English, Spanish]. Radiologia 2015;57(01):22–34
10 Chhabra A, Andreisek G, Soldatos T, et al. MR neurography: past, present, and future. AJR Am J Roentgenol 2011;197(03):583–591
11 Kim S, Choi J-Y, Huh Y-M, et al. Role of magnetic resonance imaging in entrapment and compressive neuropathy—what, where, and how to see the peripheral nerves on the musculoskeletal magnetic resonance image: part 2. Upper extremity. Eur Radiol 2007;17(02):509–522
12 Kwee RM, Chhabra A, Wang KC, Marker DR, Carrino JA. Accuracy of MRI in diagnosing peripheral nerve disease: a systematic review of the literature. AJR Am J Roentgenol 2014;203(06):1303–1309
13 Chen WC, Tsai YH, Weng HH, et al. Value of enhancement technique in 3D-T2-STIR images of the brachial plexus. J Comput Assist Tomogr 2014;38(03):335–339
14 Wendl CM, Eiglsperger J, Dendl L-M, et al. Fat suppression in magnetic resonance imaging of the head and neck region: is the two-point DIXON technique superior to spectral fat suppression? Br J Radiol 2018;91(1085):20170078
15 Ye JC. Compressed sensing MRI: a review from signal processing perspective. BMC Biomed Eng 2019;1:8
16 Kasper JM, Wadhwa V, Scott KM, Rozen S, Xi Y, Chhabra A. SHINKEI—a novel 3D isotropic MR neurography technique: technical advantages over 3DIRTSE-based imaging. Eur Radiol 2015; 25(06):1672–1677

This document was downloaded for personal use only. Unauthorized distribution is strictly prohibited.

17 Hill BJ, Padgett KR, Kalra V, et al. Gadolinium DTPA enhancement characteristics of the rat sciatic nerve after crush injury at 4.7T. AJNR Am J Neuroradiol 2018;39(01):177–183
18 Lavini C, Buiter MS, Maas M. Use of dynamic contrast enhanced time intensity curve shape analysis in MRI: theory and practice. Reports Med Imaging. 2013;6(01):71–82
19 Van der Cruyssen F, Croonenborghs TM, Renton T, et al. Magnetic resonance neurography of the head and neck: state of the art, anatomy, pathology and future perspectives. Br J Radiol 2021;94 (1119):20200798
20 Zare M, Faeghi F, Hosseini A, Ardekani MS, Heidari MH, Zarei E. Comparison between three-dimensional diffusion-weighted PSIF technique and routine imaging sequences in evaluation of peripheral nerves in healthy people. Basic Clin Neurosci 2018;9(01): 65–71
21 Chu J, Zhou Z, Hong G, et al. High-resolution MRI of the intraparotid facial nerve based on a microsurface coil and a 3D reversed fast imaging with steady-state precession DWI sequence at 3T. AJNR Am J Neuroradiol 2013;34(08):1643–1648
22 Chhabra A, Soldatos T, Subhawong TK, et al. The application of three-dimensional diffusion-weighted PSIF technique in peripheral nerve imaging of the distal extremities. J Magn Reson Imaging 2011;34(04):962–967
23 Martín Noguerol T, Barousse R. Update in the evaluation of peripheral nerves by MRI, from morphological to functional neurography [in English, Spanish]. Radiologia (Engl Ed) 2020;62(02):90–101
24 Takahara T, Hendrikse J, Yamashita T, et al. Diffusion-weighted MR neurography of the brachial plexus: feasibility study. Radiology 2008;249(02):653–660
25 Foesleitner O, Sulaj A, Sturm V, et al. Diffusion MRI in peripheral nerves: optimized *b* values and the role of non-gaussian diffusion. Radiology 2022;302(01):153–161
26 de Figueiredo E, Borgonovi AF, Doring TM. Basic concepts of MR imaging, diffusion MR imaging, and diffusion tensor imaging. Magn Reson Imaging Clin N Am 2011;19(01):1–22
27 Hiltunen J, Suortti T, Arvela S, Seppä M, Joensuu R, Hari R. Diffusion tensor imaging and tractography of distal peripheral nerves at 3 T. Clin Neurophysiol 2005;116(10):2315–2323
28 Simon NG, Lagopoulos J, Gallagher T, Kliot M, Kiernan MC. Peripheral nerve diffusion tensor imaging is reliable and reproducible. J Magn Reson Imaging 2016;43(04):962–969
29 Jeon T, Fung MM, Koch KM, Tan ET, Sneag DB. Peripheral nerve diffusion tensor imaging: overview, pitfalls, and future directions. J Magn Reson Imaging 2018;47(05):1171–1189
30 Guggenberger R, Nanz D, Bussmann L, et al. Diffusion tensor imaging of the median nerve at 3.0 T using different MR scanners: agreement of FA and ADC measurements. Eur J Radiol 2013;82 (10):e590–e596
31 Wheeler-Kingshott CAM, Cercignani M. About "axial" and "radial" diffusivities. Magn Reson Med 2009;61(05):1255–1260
32 Heckel A, Weiler M, Xia A, et al. Peripheral nerve diffusion tensor imaging: assessment of axon and myelin sheath integrity. PLoS One 2015;10(06):e0130833
33 Gallagher TA, Simon NG, Kliot M. Diffusion tensor imaging to visualize axons in the setting of nerve injury and recovery. Neurosurg Focus 2015;39(03):E10
34 Pridmore MD, Glassman GE, Pollins AC, et al. Initial findings in traumatic peripheral nerve injury and repair with diffusion tensor imaging. Ann Clin Transl Neurol 2021;8(02):332–347
35 Holmes SA, Karapanagou A, Staffa SJ, et al. DTI and MTR measures of nerve fiber integrity in pediatric patients with ankle injury. Front Pediatr 2021;9(September):656843
36 Wang C-K, Jou I-M, Huang H-W, et al. Carpal tunnel syndrome assessed with diffusion tensor imaging: comparison with electrophysiological studies of patients and healthy volunteers. Eur J Radiol 2012;81(11):3378–3383
37 Chhabra A, Thakkar RS, Andreisek G, et al. Anatomic MR imaging and functional diffusion tensor imaging of peripheral nerve tumors and tumorlike conditions. AJNR Am J Neuroradiol 2013; 34(04):802–807
38 Bruno F, Arrigoni F, Mariani S, et al. Application of diffusion tensor imaging (DTI) and MR-tractography in the evaluation of peripheral nerve tumours: state of the art and review of the literature. Acta Biomed 2019;90(5-S):68–76
39 Liu C, Li HW, Wang L, et al. Optimal parameters and location for diffusion tensor imaging in the diagnosis of carpal tunnel syndrome: a meta-analysis. Clin Radiol 2018;73(12):1058.e11–1058. e19
40 Acer N, Turgut M. Evaluation of brachial plexus using combined stereological techniques of diffusion tensor imaging and fiber tracking. J Brachial Plex Peripher Nerve Inj 2019;14(01):e16–e23
41 Triadyaksa P, Oudkerk M, Sijens PE. Cardiac $T_2{}^*$ mapping: techniques and clinical applications. J Magn Reson Imaging 2020;52 (05):1340–1351
42 Hesper T, Neugroda C, Schleich C, et al. T2*-mapping of acetabular cartilage in patients with femoroacetabular impingement at 3 Tesla: comparative analysis with arthroscopic findings. Cartilage 2018;9(02):118–126
43 Hiwatashi A, Togao O, Yamashita K, et al. Simultaneous MR neurography and apparent T2 mapping in brachial plexus: evaluation of patients with chronic inflammatory demyelinating polyradiculoneuropathy. Magn Reson Imaging 2019; 55:112–117
44 Eguchi Y, Enomoto K, Sato T, et al. Simultaneous MR neurography and apparent T2 mapping of cervical nerve roots before microendoscopic surgery to treat patient with radiculopathy due to cervical disc herniation: preliminary results. J Clin Neurosci 2020; 74:213–219
45 Sollmann N, Weidlich D, Cervantes B, et al. T2 mapping of lumbosacral nerves in patients suffering from unilateral radicular pain due to degenerative disc disease. J Neurosurg Spine 2019(Feb 22):1–9
46 Sollmann N, Weidlich D, Klupp E, et al. T2 mapping of the distal sciatic nerve in healthy subjects and patients suffering from lumbar disc herniation with nerve compression. MAGMA 2020; 33(05):713–724
47 Preisner F, Behnisch R, Foesleitner O, et al. Reliability and reproducibility of sciatic nerve magnetization transfer imaging and T2 relaxometry. Eur Radiol 2021;31(12): 9120–9130
48 Chappell KE, Robson MD, Stonebridge-Foster A, et al. Magic angle effects in MR neurography. AJNR Am J Neuroradiol 2004;25(03): 431–440
49 Kästel T, Heiland S, Bäumer P, Bartsch AJ, Bendszus M, Pham M. Magic angle effect: a relevant artifact in MR neurography at 3T? AJNR Am J Neuroradiol 2011;32(05):821–827
50 Sakai T, Aoki Y, Watanabe A, Yoneyama M, Ochi S, Miyati T. Functional assessment of lumbar nerve roots using coronal-plane single-shot turbo spin-echo diffusion tensor imaging. Magn Reson Med Sci 2020;19(02):159–165
51 Martín-Noguerol T, Montesinos P, Barousse R, Luna A. *RadioGraphics* update: Functional MR neurography in evaluation of peripheral nerve trauma and postsurgical assessment. Radiographics 2021;41(02):E40–E44
52 De Paepe KN, Higgins DM, Ball I, Morgan VA, Barton DP, deSouza NM. Visualizing the autonomic and somatic innervation of the female pelvis with 3D MR neurography: a feasibility study. Acta Radiol 2020;61(12):1668–1676
53 Muniz Neto FJ, Kihara Filho EN, Miranda FC, Rosemberg LA, Santos DCB, Taneja AK. Demystifying MR neurography of the lumbosacral plexus: from protocols to pathologies. BioMed Res Int 2018; 2018:9608947

This document was downloaded for personal use only. Unauthorized distribution is strictly prohibited.